Gas-Phase Chemistry

Synthesis of Polycyclic Aromatic Hydrocarbons by Phenyl Addition–Dehydrocyclization: The Third Way

Long Zhao, Matthew B. Prendergast, Ralf I. Kaiser,* Bo Xu, Utuq Ablikim, Musahid Ahmed,* Bing-Jian Sun, Yue-Lin Chen, Agnes H. H. Chang,* Rana K. Mohamed, and Felix R. Fischer*

Abstract: Polycyclic aromatic hydrocarbons (PAHs) represent the link between resonance-stabilized free radicals and carbonaceous nanoparticles generated in incomplete combustion processes and in circumstellar envelopes of carbon rich asymptotic giant branch (AGB) stars. Although these PAHs resemble building blocks of complex carbonaceous nanostructures, their fundamental formation mechanisms have remained elusive. By exploring these reaction mechanisms of the phenyl radical with biphenyl/naphthalene theoretically and experimentally, we provide compelling evidence on a novel phenyl-addition/dehydrocyclization (PAC) pathway leading to prototype PAHs: triphenylene and fluoranthene. PAC operates efficiently at high temperatures leading through rapid molecular mass growth processes to complex aromatic structures, which are difficult to synthesize by traditional pathways such as hydrogen-abstraction/acetylene-addition. The elucidation of the fundamental reactions leading to PAHs is necessary to facilitate an understanding of the origin and evolution of the molecular universe and of carbon in our galaxy.

Introduction

For decades, polycyclic aromatic hydrocarbons (PAHs)—organic molecules featuring laterally fused benzene rings[1]—have been at the center of attention as prospective candidates to untangle the molecular carriers of the unidentified infrared (UIR) emissions[2] and of the diffuse interstellar bands (DIBs).[2] These surveys propose that PAHs may encompass up to 20% of the galactic carbon budget[3] and act as a link between resonantly stabilized free radicals (RSFRs)[4] and carbonaceous nanoparticles in interstellar and circumstellar environments.[5] The detection of PAHs in carbonaceous chondrites such as Murchison along with $^{13}C/^{12}C$ isotopic analyses advocates an extraterrestrial origin of PAHs[1,6] with

fundamental astrochemical models of PAH synthesis borrowed from the combustion community.[7] The hydrogen-abstraction/acetylene-addition (HACA) mechanism has been suggested to be important in the formation of PAHs in outflows of carbon-rich asymptotic giant branch (AGB) stars[8] and in the combustion of fossil fuel.[9] A repetitive sequence of an abstraction of a hydrogen atom from the aromatic hydrocarbon followed by an addition of acetylene (C_2H_2) prior to cyclization and aromatization lead to PAHs carrying up to four fused benzene rings—naphthalene ($C_{10}H_8$),[7a] phenanthrene ($C_{14}H_{10}$)[7c,10] and pyrene ($C_{16}H_{10}$)[11]—can be synthesized at high temperatures involving HACA. Recently, the hydrogen-abstraction/vinylacetylene-addition (HAVA) mechanism has been invoked since naphthalene ($C_{10}H_8$),[12] phenanthrene ($C_{14}H_{10}$), and anthracene ($C_{14}H_{10}$)[13] were shown to be synthesized by barrier-less collisions of phenyl ($C_6H_5^{\cdot}$) and naphthyl ($C_{10}H_7^{\cdot}$) radicals with vinylacetylene (C_4H_4) through ring annulation at temperatures as low as 10 K.

Despite their potential in synthesizing PAHs in extreme environments, both the HAVA and HACA mechanisms have come under scrutiny, since flame data and recent models infer that a stepwise addition of acetylene is too slow to reproduce the quantified mass fractions of PAHs in combustion flames and in circumstellar environments.[14] Koshi et al.[15] along with Li et al.[16] postulated that an overlooked phenyl-addition/dehydrocyclization (PAC) mechanism may result in a rapid synthesis of PAHs. This hypothetical PAC route involves an addition of phenyl to an aromatic hydrocarbon. This is followed by hydrogen loss and successive dehydrogenation succeeded by cyclization along with another hydrogen atom loss accompanied by aromatization (Figure 1). However, the validity of PAC has remained uncharted, since not a single experimental study could substantiate to what extent

[*] Dr. L. Zhao, Dr. M. B. Prendergast, Prof. R. I. Kaiser,
Dr. R. K. Mohamed
Department of Chemistry, University of Hawaii at Manoa
Honolulu, Hawaii, 96822 (USA)
E-mail: ralfk@hawaii.edu

Dr. B. Xu, Dr. U. Ablikim, Dr. M. Ahmed
Chemical Sciences Division, Lawrence Berkeley National Laboratory
Berkeley, CA 94720 (USA)
E-mail: mahmed@lbl.gov

Dr. B. J. Sun, Dr. Y. L. Chen, Prof. A. H. H. Chang
Department of Chemistry, National Dong Hwa University
Shoufeng, Hualien 974 (Taiwan, ROC)
E-mail: hhchang@gms.ndhu.edu.tw

Dr. R. K. Mohamed, Prof. F. R. Fischer
Department of Chemistry, University of California Berkeley
Berkeley, CA 94720 (USA)
E-mail: ffischer@berkeley.edu

Prof. F. R. Fischer
Materials Sciences Division, Lawrence Berkeley National Laboratory
Berkeley, CA 94720 (USA)

Prof. F. R. Fischer
Kavli Energy Nano Sciences Institute at the University of California
Berkeley and the Lawrence Berkeley National Laboratory
Berkeley, CA 94720 (USA)

Supporting information and the ORCID identification number(s) for the author(s) of this article can be found under:
https://doi.org/10.1002/anie.201909876.
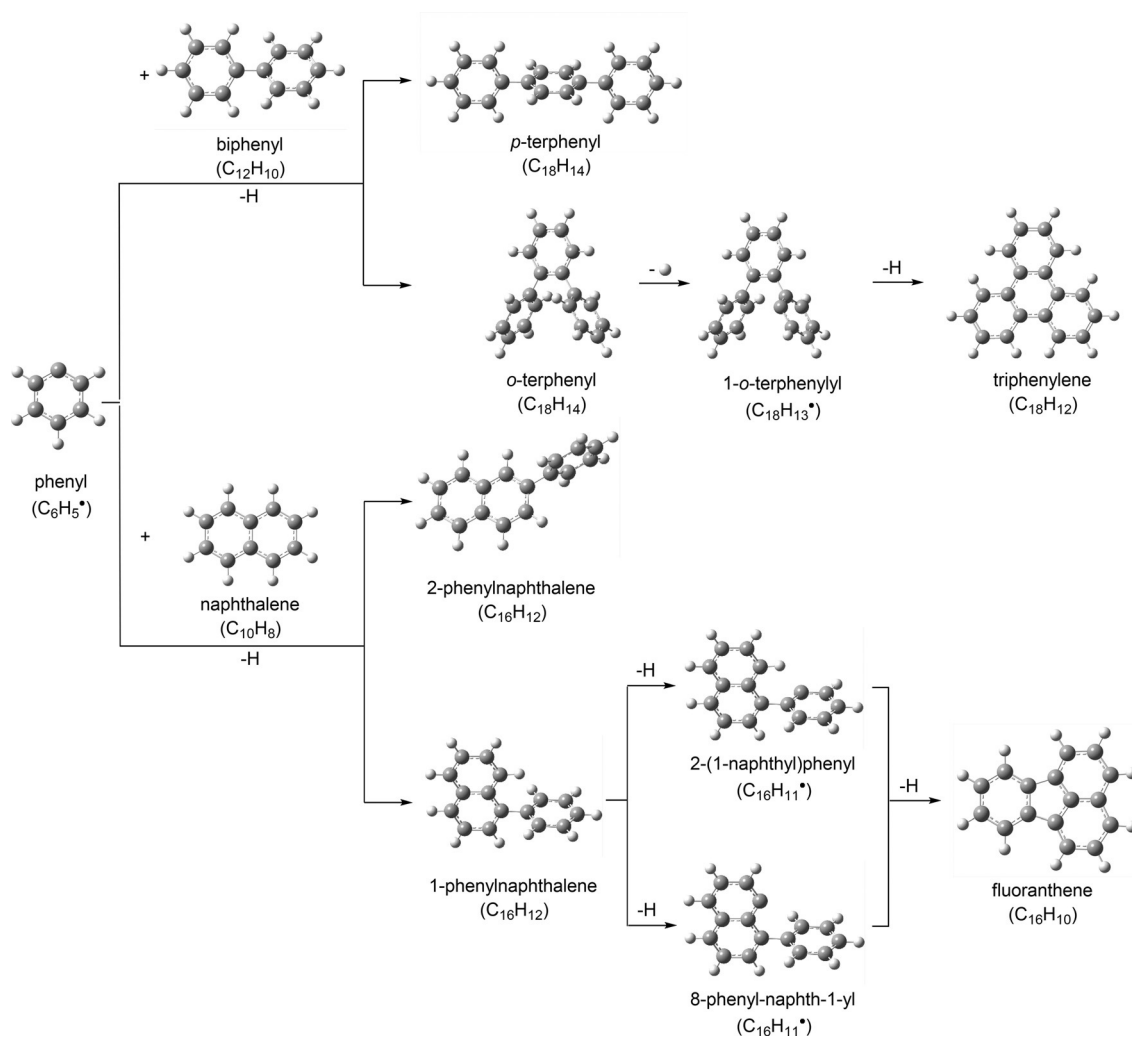
Figure 1. Postulated reactions leading to PAH formation through the phenyl addition/dehydro-cyclization (PAC) mechanism. Carbon and hydrogen atoms are color coded gray and white, respectively.

PAHs can form since all mechanisms, HACA, HAVA, and PAC, operate simultaneously in combustion environments. This complexity requires a systematic elucidation of the fundamental elementary reactions[17] involved in the PAC route.

Herein, we reveal the facile gas phase synthesis of two prototype PAHs, fluoranthene ($C_{16}H_{10}$) and triphenylene ($C_{18}H_{12}$), by PAC in high temperature environments (Figure 1). This is achieved by first disentangling the previously elusive chemistry of the elementary reactions of phenyl ($C_6H_5\cdot$) with biphenyl ($C_6H_5–C_6H_5$) and naphthalene ($C_{10}H_8$) forming triphenylene ($C_{18}H_{12}$) and fluoranthene ($C_{16}H_{10}$), respectively. Then, we trace the reactivity of a prototype radical intermediate in PAC—2-(1-naphthyl)phenyl ($C_{16}H_{11}\cdot$) and provide critical evidence on the role of key hydrocarbon radicals. These findings suggest PAC as a third way, besides HACA and HAVA, to efficiently synthesize PAHs, serving as building blocks of two- and three-dimensional aromatic structures in combustion flames and in circumstellar envelopes. Briefly, a high temperature chemical reactor was used to form fluoranthene ($C_{16}H_{10}$) and triphenylene ($C_{18}H_{12}$) by

the reactions of the phenyl radical with naphthalene ($C_{10}H_8$) and biphenyl ($C_6H_5–C_6H_5$), respectively; second, ring closure of the 2-(1-naphthyl)phenyl radical ($C_{16}H_{11}\cdot$) followed by hydrogen loss and aromatization to fluoranthene ($C_{16}H_{10}$) highlights the key role of aromatic radical intermediates in the PAC mechanism. All products were detected isomer-specifically through fragment-free photoionization in a molecular beam by tunable vacuum ultraviolet light in tandem with the identification of the ionized molecules in a reflectron time-of-flight mass spectrometer (Supporting Information).

Results and Discussion

Mass Spectra

Representative mass spectra recorded at a photoionization energy of 9.50 eV for the reactions of biphenyl and naphthalene with the phenyl radical are displayed in Figure 2. A comparison of these data with reference spectra obtained for biphenyl and naphthalene seeded in non-reactive helium gas
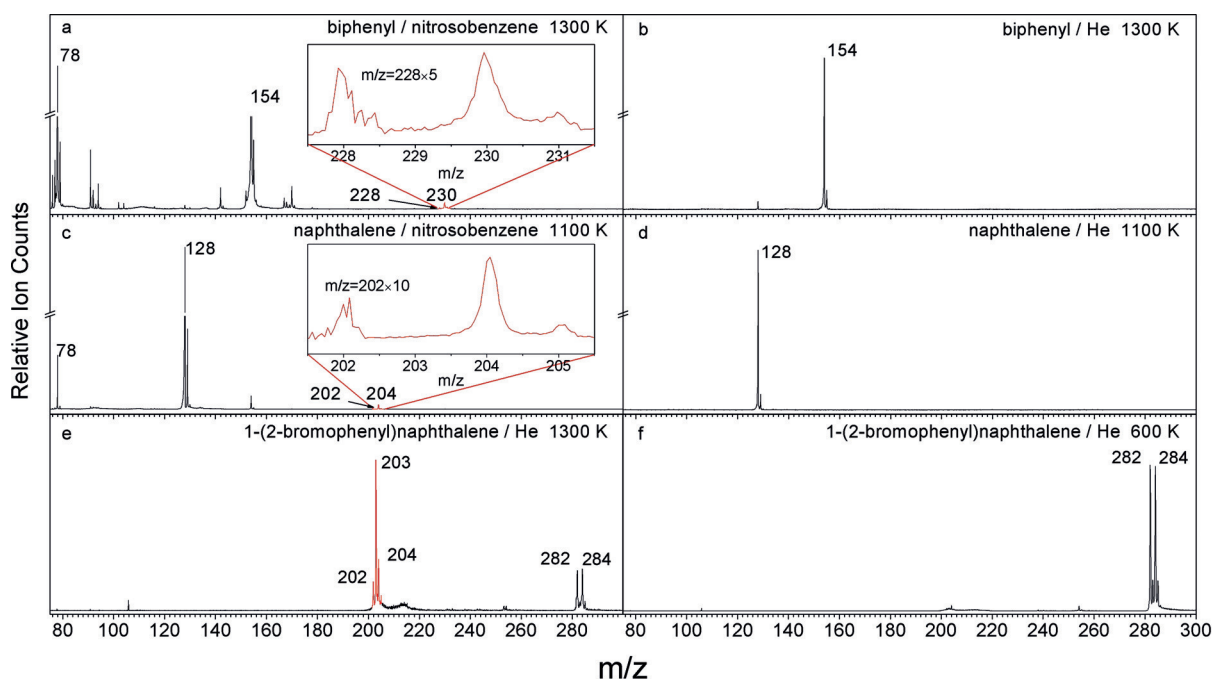
Figure 2. Comparison of photoionization mass spectra recorded at a photoionization energy of 9.50 eV. a) Biphenyl ($C_{12}H_{10}$)–nitrosobenzene (C_6H_5NO); the insert highlights the ion signals at $m/z = 228$. b) Biphenyl ($C_{12}H_{10}$)–helium (He). (c) Naphthalene ($C_{10}H_8$)–nitrosobenzene (C_6H_5NO); the insert highlights the ion signals at $m/z = 202$. d) Naphthalene ($C_{10}H_8$)–helium; pyrolysis of 1-(2-bromophenyl) naphthalene at 1300 K e) and 600 K f). Mass peaks of the newly formed species of interest are highlighted in red. The inserts magnify sections of the mass spectra.

provides evidence on the synthesis of molecules with the molecular formula $C_{18}H_{12}$ (228 amu) and $C_{18}H_{14}$ (230 amu) (Figure 2 a) as well as of $C_{16}H_{10}$ (202 amu) and $C_{16}H_{12}$ (204 amu) (Figure 2 c); these species are absent in the control experiments (Figures 2 b,d). The following analysis allows us to gauge the reactivity of the 2-(1-naphthyl)phenyl radical intermediate ($C_{16}H_{11}^{\bullet}$) (Figures 2 e,f). At 600 K, the 1-(2-bromophenyl)naphthalene precursor molecule is assigned through the molecular ion peaks at $m/z = 282$ ($C_{16}H_{11}^{79}Br$), 283 ($^{13}CC_{15}H_{11}^{79}Br$), 284 ($C_{16}H_{11}^{81}Br$), and 285 ($^{13}CC_{15}H_{11}^{81}Br$) (Figure 2 f). When the temperature is increased to 1300 K, new ion counts arise at $m/z = 202$ ($C_{16}H_{10}^+$), 203 ($C_{16}H_{11}^+/$ $^{13}CC_{15}H_{10}^+$), and 204 ($C_{16}H_{12}^+$) (Figure 2 e). To further identify the nature of the isomers formed in these systems, photoionization efficiency (PIE) curves, which record the intensities of an ion at a well-defined mass-to-charge ratio versus the photon energy, were collected between 7.5 to 10.0 eV. The experimentally recorded PIE curves are fit with a linear combination of known PIE calibration curves of distinct structural isomers to identify which molecule(s) is(are) synthesized.
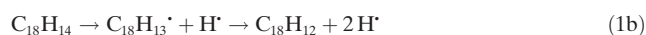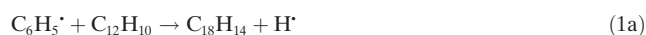
Photoionization Efficiency (PIE) Curves

In the biphenyl–phenyl system, accounting for the molecular weight of the reactants ($C_{12}H_{10}$, 154 amu; $C_6H_5^{\bullet}$, 77 amu) and the products ($C_{18}H_{14}$, 230 amu; H, 1 amu), molecules with the formula $C_{18}H_{14}$ can be linked to reaction products of the elementary reaction of biphenyl with the phenyl radical

(Figures 2 a,b) with ion count at $m/z = 231$ connected to ^{13}C-substituted counterpart of $m/z = 230$ ($^{13}CC_{17}H_{14}$) [reaction (1a)]. Ion counts at $m/z = 230$ and 231 are absent in the control experiment suggesting that signals at these mass-to-charge ratios originate from reaction between the phenyl radical and biphenyl. Ion counts at $m/z = 77$ ($C_6H_5^+$), 78 ($C_6H_6^+/C_5^{13}CH_5^+$), and 79 ($C_5^{13}CH_6^+$) are also observable; they are attributed to phenyl ($C_6H_5^{\bullet}$), benzene (C_6H_6), and ^{13}C-benzene ($C_5^{13}CH_6$). Signal is also detectable at $m/z = 228$, which can be associated with two subsequent hydrogen atom losses and dehydrogenation from $C_{18}H_{14}$ via $C_{18}H_{13}^{\bullet}$ to $C_{18}H_{12}$ [reaction (1b)]. To summarize, the analysis of the mass spectra alone reveals that the reaction of the biphenyl ($C_{12}H_{10}$) with phenyl ($C_6H_5^{\bullet}$) synthesizes hydrocarbon molecule(s) with the molecular formulae $C_{18}H_{12}$ and $C_{18}H_{14}$. To identify the structural isomers formed, the PIE curves recorded at $m/z = 228$, 230, and 231 are analyzed (Figures 3 a–c). For $m/z = 230$ and 231, the experimental PIE curves depict onsets of the ion counts at 7.85 ± 0.05 eV, which agree very well with the adiabatic ionization energy of p-terphenyl of 7.80 ± 0.03 eV.[18] After scaling, both PIE graphs at $m/z = 230$ and 231 are identical and can be replicated with the PIE curve of the p-terphenyl isomer (Supporting Information and Figures 3 b,c) amplifying that signal at $m/z = 231$ originates from ^{13}C-labeled p-terphenyl ($^{13}CC_{17}H_{14}$). Most important, after scaling, the PIE curve at $m/z = 228$ does not overlap with the PIE curve at $m/z = 230$ suggesting that signal at $m/z = 228$ does not originate from fragments of $m/z = 230$. Herein, the PIE curve at $m/z = 228$ can be reproduced with a PIE curve of triphenylene ($C_{18}H_{12}$) (Supporting Information and Fig-
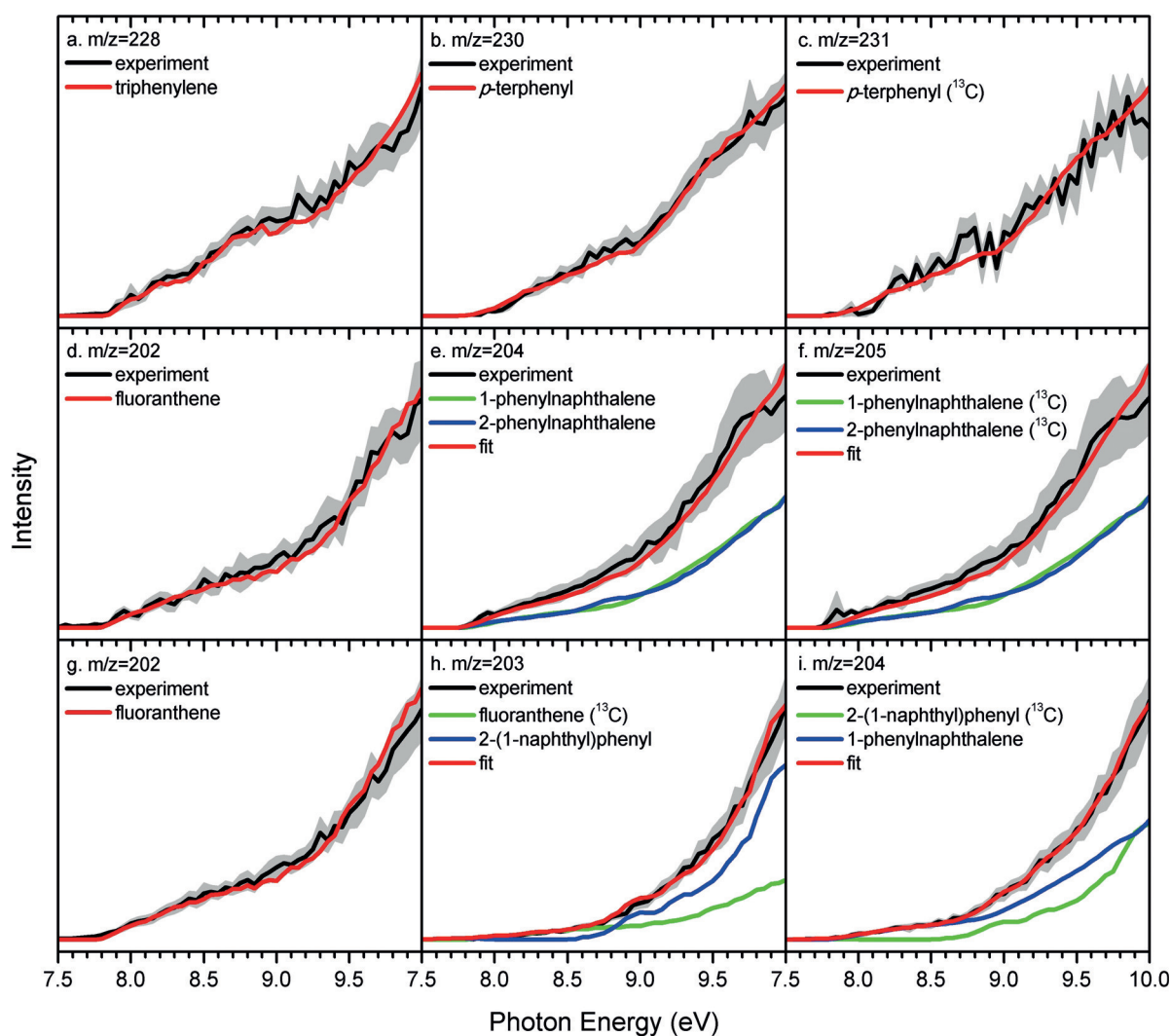
Figure 3. Photoionization efficiency (PIE) curves: a)–c): phenyl ($C_6H_5^\bullet$)–biphenyl ($C_{12}H_{10}$); d)–f): phenyl ($C_6H_5^\bullet$)–naphthalene ($C_{10}H_8$); g)–i): 1-(2-bromophenyl)naphthalene (1300 K). Black: experimental PIE curves; blue/green/red: reference PIE curves; the red line resembles the overall fit.

ure 3a). The experimentally determined onset of ion counts at $m/z = 228$ at 7.85 ± 0.05 eV corresponds to the adiabatic ionization energy of triphenylene of 7.89 ± 0.04 eV.[19] Consequently, our investigations reveal that in the phenyl–biphenyl system, molecular mass growth processes account for the formation of *p*-terphenyl ($C_{18}H_{14}$) and of triphenylene ($C_{18}H_{12}$) formed through reactions (1a) and (1b), respectively.
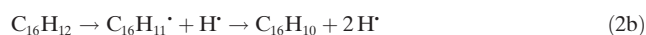
$$C_6H_5^\bullet + C_{12}H_{10} \rightarrow C_{18}H_{14} + H^\bullet \tag{1a}$$

$$C_{18}H_{14} \rightarrow C_{18}H_{13}^\bullet + H^\bullet \rightarrow C_{18}H_{12} + 2\,H^\bullet \tag{1b}$$

In the naphthalene–phenyl system, considering the molecular weight of the reactants ($C_{10}H_8$, 128 amu; $C_6H_5^\bullet$, 77 amu) and the products ($C_{16}H_{12}$, 204 amu; H, 1 amu), molecules with the formula $C_{16}H_{12}$ are identified (Figures 2c,d) with ion count at $m/z = 205$ correlated with the ^{13}C-substituted counterpart of $m/z = 204$ ($^{13}CC_{15}H_{12}$) [reaction (2a)]. Since the ion counts at $m/z = 204$ and 205 cannot be detected in the control experiment, signals at both mass-to-

charge ratios are linked to the reaction between the phenyl radical and naphthalene. Signal can be monitored at $m/z = 202$ as well. This is linked to two successive hydrogen atom losses and dehydrogenation from $C_{16}H_{12}$ yielding ultimately $C_{16}H_{10}$ [reaction (2b)]. Ion counts at $m/z = 77$ ($C_6H_5^+$), 78 ($C_6H_6^+/C_5^{13}CH_5^+$), 79 ($C_5^{13}CH_6^+$), 128 ($C_{10}H_8^+$), and 129 ($^{13}CC_9H_8^+$) can also be detected. The corresponding neutrals are phenyl ($C_6H_5^\bullet$), benzene (C_6H_6), ^{13}C-benzene ($^{13}CC_5H_6$), naphthalene ($C_{10}H_8$), and ^{13}C- naphthalene ($^{13}CC_9H_8$). Thus, the mass spectra reveal that the reaction of naphthalene ($C_{10}H_8$) with phenyl ($C_6H_5^\bullet$) synthesizes hydrocarbon molecules with the molecular formulae $C_{16}H_{12}$ and $C_{16}H_{10}$. To assign the isomers, the PIE curves at $m/z = 202$, 204, and 205 are examined (Figures 3d–f). At $m/z = 204$ and 205, both PIE graphs are superimposable after scaling and can be fit with a linear combination of the reference PIE graphs of 1- and 2-phenylnaphthalene (Supporting Information). Hence the signal at $m/z = 205$ originates from $^{13}CC_{15}H_{12}$. The PIE calibration curves for 1- and 2-phenylnaphthalene isomers are nearly superimposable, and hence it is not feasible to

determine accurate branching ratios of these isomers in the phenyl-naphthalene system. On the other hand, the PIE curves at $m/z = 202$ and 204 are distinct; data at $m/z = 202$ can be replicated with the PIE graph of fluoranthene ($C_{16}H_{10}$) (Supporting Information). The experimental onset of the ion counts at $m/z = 202$ at 7.85 ± 0.05 eV correlates nicely with the adiabatic ionization energy of fluoranthene of 7.90 ± 0.10 eV.[20] Altogether, the experiments propose that in the phenyl–naphthalene system, 1- and/or 2-phenylnaphthalene ($C_{16}H_{12}$) along with fluoranthene ($C_{16}H_{10}$) are formed.

$$C_6H_5{}^{\cdot} + C_{10}H_8 \rightarrow C_{16}H_{12} + H^{\cdot} \qquad (2a)$$

$$C_{16}H_{12} \rightarrow C_{16}H_{11}{}^{\cdot} + H^{\cdot} \rightarrow C_{16}H_{10} + 2\,H^{\cdot} \qquad (2b)$$

Considering the 1-(2-bromophenyl)naphthalene system, signal at $m/z = 282$ ($C_{16}H_{11}{}^{79}Br$), 283 ($^{13}CC_{15}H_{11}{}^{79}Br$), 284 ($C_{16}H_{11}{}^{81}Br$), and 285 ($^{13}CC_{15}H_{11}{}^{81}Br$) is associated with the precursor molecules and their ^{13}C substituted counterparts. A detailed analysis of the PIE graphs in the 1300 K experiment (Figures 3g–i) reveals that ion counts at $m/z = 202$ are associated with fluoranthene ($C_{16}H_{10}$). The reference curves match the experimental data exceptionally well and reveal an onset of 7.80 ± 0.05 eV, which correlates nicely with the adiabatic ionization energy of fluoranthene of 7.90 ± 0.10 eV.[20] The PIE graph at $m/z = 203$ ($C_{16}H_{11}{}^{+}/{}^{13}CC_{15}H_{10}{}^{+}$) can be replicated by a linear combination of the reference curves of ^{13}C- fluoranthene and the 2-(1-naphthyl)phenyl radical. Finally, the signal at $m/z = 204$ can be explained by 1-phenylnaphthalene formed, for example, by hydrogen abstraction of the 2-(1-naphthyl)phenyl radical. In summary, our investigations reveal that the 2-(1-naphthyl)phenyl radical, a key intermediate in the PAC mechanism, undergoes isomerization through ring closure followed by atomic hydrogen loss yielding eventually fluoranthene ($C_{16}H_{10}$) [reaction (3), Figure 1].

$$C_{16}H_{11}{}^{\cdot} \rightarrow C_{16}H_{10} + H^{\cdot} \qquad (3)$$

Reaction Mechanisms
Formation of Triphenylene

The present study reveals that two prototype PAHs carrying three and four benzene rings—triphenylene ($C_{18}H_{12}$) and fluoranthene ($C_{16}H_{10}$)—are synthesized within the phenyl–naphthalene and phenyl–biphenyl systems, respectively, in the gas phase. To elucidate the underlying reaction mechanisms, we combined these findings with electronic structure calculations. Considering the reaction of the phenyl radical with biphenyl [reaction (1a)], the phenyl radical can add to the *ortho* (*o*-), *meta* (*m*-), and/or *para* (*p*-) position of the phenyl moiety of the biphenyl molecule through a barrier up to 27 kJ mol^{-1} (Figures 4a/b). The resulting doublet radical intermediates **i1** to **i3** undergo hydrogen atom loss forming *o*-, *m*-, and *p*-terphenyl. Secondary reactions of atomic hydrogen and/or phenyl radicals with *o*-terphenyl lead, through hydrogen abstraction, to the 1-*o*-terphenylyl (**i4**) radical, which can undergo facile cyclization to the doublet intermediate radical **i5**. Accompanied by
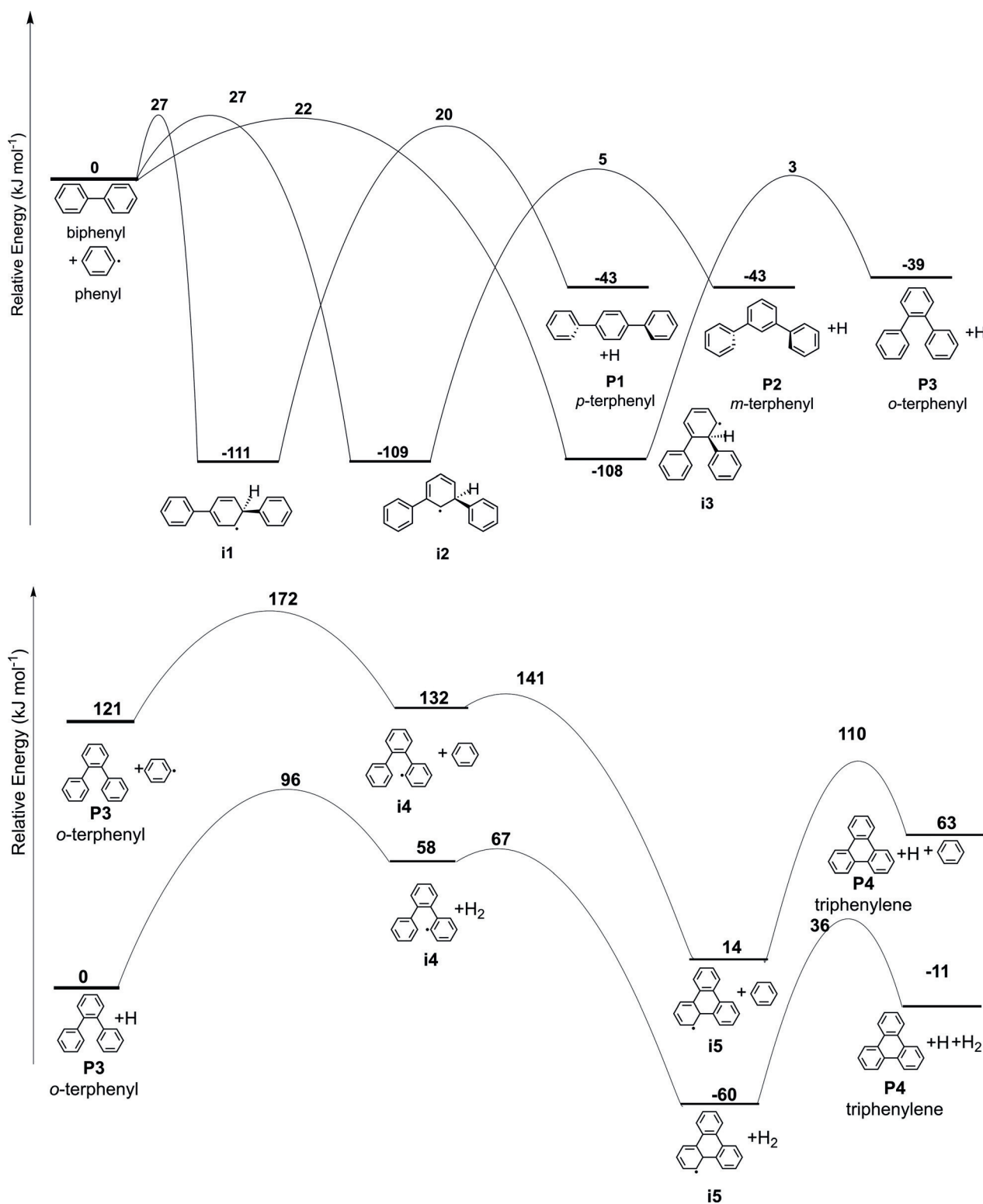
aromatization, the latter undergoes unimolecular decomposition through atomic hydrogen loss, forming triphenylene in overall exergic reactions. Considering the heights of the barriers along with the overall reaction energies, the reaction of phenyl with *o*-terphenyl is favorable both kinetically and thermodynamically. These computations assist in rationalizing our experimental observations of the formation of *p*-terphenyl ($C_{18}H_{14}$) and triphenylene ($C_{18}H_{12}$). The initial replacement of a hydrogen atom by a phenyl group in the biphenyl reactant represents a prototype of an aromatic radical substitution reaction (S_R). This reaction favors the addition of the radical reactant to the *o*- and *p*-position of the phenyl moiety[21] followed by atomic hydrogen loss leading to *o*- and *p*-terphenyl, but not to *m*-terphenyl. The *p*-terphenyl was observed experimentally; the absence of *o*-terphenyl, but the identification of triphenylene suggests an efficient conversion through dehydrogenation and cyclization of *o*-terphenyl to triphenylene (Figure 1) thus demonstrating the unique capability of PAC to synthesize triphenylene.

Formation of Fluoranthene

In the phenyl–naphthalene system (Figure 5a), the phenyl radical adds to the C1 or C2 carbon atom of naphthalene yielding **i6** and **i7** doublet radical intermediates. These emit atomic hydrogen yielding 1-/2-phenylnaphthalene, respectively, in overall exergic reactions. Secondary reaction of atomic hydrogen and/or phenyl radicals can abstract atomic hydrogen from 1-phenylnaphthalene. The hydrogen abstractions at the *ortho* positions of the phenyl and at the C8 carbon atom of the naphthalene moieties are critical to highlight. These abstractions lead to 2-(1-naphthyl)phenyl (**i8**) and 8-phenyl-naphth-1-yl (**i9**). Both the 2-(1-naphthyl)phenyl and 8-phenyl-naphth-1-yl radicals undergo cyclization to 1- and 7-H-fluoranthenyl **i10** and **i11**, respectively. Unimolecular decomposition of these intermediates through atomic hydrogen loss accompanied by aromatization forms fluoranthene (Figure 5b). These predictions correlate well with our experimental findings and rationalize the identification of fluoranthene by PAC.

Conclusion

To conclude, our experimental data identified fluoranthene ($C_{16}H_{10}$) and triphenylene ($C_{18}H_{12}$) as key reaction products in the phenyl–biphenyl and phenyl–naphthalene systems with electronic structure calculations revealing the critical involvement of the previously elusive PAC mechanism. Since the initial addition of the phenyl radical to benzene and naphthalene along with the hydrogen abstraction from *o*-terphenyl and 1-phenylnaphthalene involve barriers of at least 21 kJ mol^{-1}, high temperature conditions in combustion processes and circumstellar envelopes of carbon stars, are essential to efficient mass growth processes to PAHs through PAC. The 18π aromatic triphenylene ($C_{18}H_{12}$)—a benchmark of a fully benzenoid PAH—and fluoranthene ($C_{16}H_{10}$)—a prototype of a non-alternant PAH—represent key molecular building blocks in molecular

17446 www.angewandte.org

© 2019 Wiley-VCH Verlag GmbH & Co. KGaA, Weinheim

Angew. Chem. Int. Ed. **2019**, *58*, 17442 – 17450

Figure 4. a. Potential energy surface (PES) for the reaction of phenyl ($C_6H_5\cdot$) with biphenyl ($C_{12}H_{10}$). **b.** Potential energy surface (PES) for the formation of triphenylene ($C_{18}H_{12}$) by hydrogen atom abstraction, cyclization, and hydrogen atom elimination.

mass growth processes of two- and three-dimensional PAHs. These pathways may be involved in the formation of 2D and 3D nanostructures with buckminsterfullerene (C_{60}) detected in hydrocarbon flames[22] and toward the planetary nebula TC

1 (Scheme 1).[23] Overall, our findings establish a rigorous framework promoting PAC as a third way to synthesize PAHs by efficient molecular mass growth processes. In particular, the incorporation of a five-membered ring in PAHs such as
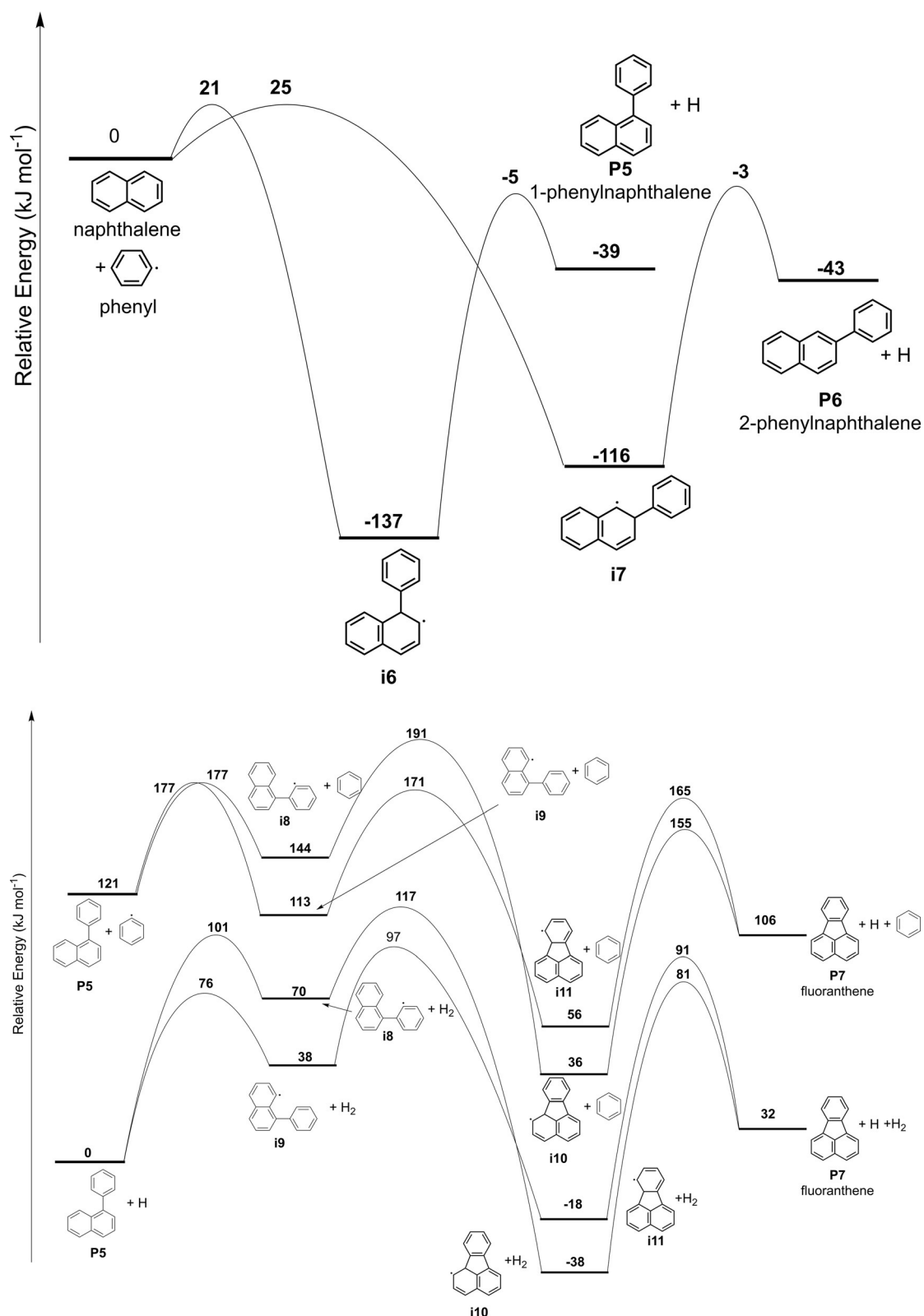
Figure 5. **a.** Potential energy surface (PES) for the reaction of phenyl ($C_6H_5^\bullet$) with naphthalene ($C_{10}H_8$). **b.** Potential energy surface (PES) for the formation of fluoranthene ($C_{16}H_{10}$) by hydrogen atom abstraction, cyclization, and hydrogen atom elimination.

fluoranthene, which has a dipole moment of 0.34 Debye, could aid in the detection of an individual PAH in the gas phase interstellar medium through its rotational spectrum exploiting the atacama large millimeter/ submillimeter array (ALMA) thus transforming how we think about the origin and evolution of carbonaceous matter in the Universe.[24]

Circumcoronene
$C_{54}H_{18}$

pentabenzocorannulene
$C_{40}H_{20}$

buckminsterfullerene
(C_{60})
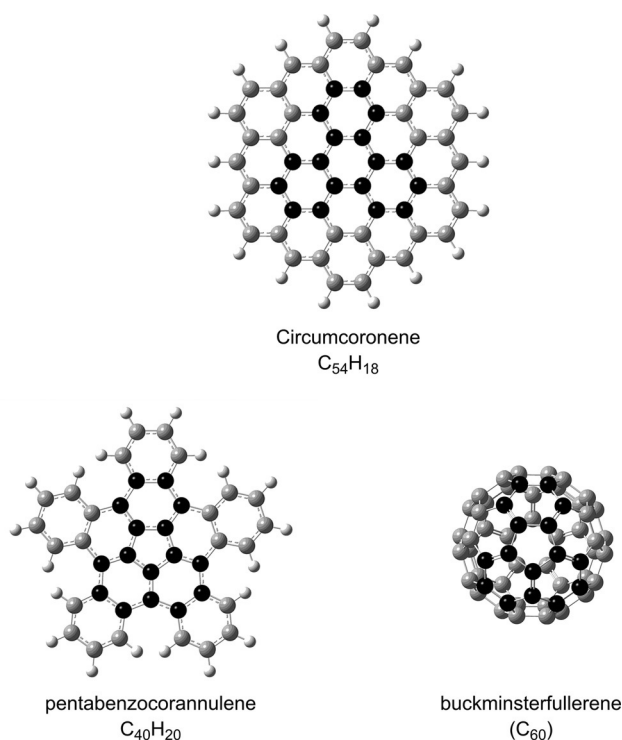
Scheme 1. Fluoranthene ($C_{16}H_{10}$) and triphenylene ($C_{18}H_{12}$) as molecular building blocks in two- and three-dimensional PAHs and fullerenes: circumcoronene ($C_{54}H_{18}$), pentabenzocorannulene ($C_{40}H_{20}$), and buckminsterfullerene (C_{60}).

Methods

Experimental: The experiments were carried out at the Chemical Dynamics Beamline (9.0.2) of the Advanced Light Source utilizing a resistively-heated silicon-carbide (SiC) chemical reactor interfaced to a molecular beam apparatus operated with a Wiley-McLaren reflectron time-of-flight mass spectrometer (Re-TOF-MS).[7a,b,11–13,25] The chemical reactor mimics the high temperature conditions present in combustion flames and in circumstellar envelopes of carbon stars. Phenyl radicals (C_6H_5·) were prepared in situ by pyrolysis of the nitrosobenzene precursor (C_6H_5NO; Sigma-Aldrich) with the biphenyl and naphthalene reactants provided by Sigma-Aldrich. The reactants were seeded in helium carrier gas (0.394 ± 0.005 atm). In the pyrolysis experiments, custom synthesized 1-(2-bromophenyl)naphthalene alone was seeded in the helium carrier gas at 0.394 ± 0.005 atm (Supporting Information). The temperature of the SiC tube was monitored using a Type-C thermocouple and was maintained at 1300 ± 10 K (nitrosobenzene/biphenyl; 1-(2-bromophenyl)-naphthalene) and 1100 ± 10 K (nitrosobenzene/naphthalene). The products formed in the reactor were expanded supersonically and passed through a 2 mm diameter skimmer located 10 mm downstream of the pyrolytic reactor and enter into the main chamber, which houses the Re-TOF-MS. The quasi-continuous tunable vacuum ultraviolet (VUV) light from the Advanced Light Source intercepted the neutral molecular beam perpendicularly in the extraction region of a Wiley-McLaren RE-TOF-MS. VUV single photon ionization is essentially a fragment-free ionization technique and hence is characterized as a soft ionization method compared to electron impact ionization, the latter leading to excessive fragmentation of the parent ion.[26] The ions formed by photoionization are extracted and eventually detected by a microchannel plate detector. Photoionization efficiency (PIE) curves, which report ion counts as a function of photon energy with a step interval of 0.05 eV at a well-defined mass-

to-charge ratio (m/z), were produced by integrating the signal recorded at the specific m/z for the species of interest. Reference (blank) experiments were also conducted by expanding helium carrier gas into the resistively-heated SiC tube without seeding the reactants in nitrosobenzene. To identify the products of interest observed in this work, PIE calibration curves for 1-phenylnaphthalene, 2-phenylnaphthalene, fluoranthene, o-terphenyl, m-terphenyl, p-terphenyl, and triphenylene (Sigma-Aldrich) were collected (Supporting Information). It is important to note that in blank experiments of nitrosobenzene seeded in helium carrier gas conducted at identical temperatures and pressures as the current experiments, naphthalene, triphenylene, or fluoranthene are not formed.[7a]

Computational: The synthetic routes to triphenylene and fluoranthene are explored by electronic structure calculations. Along these routes, reactants, intermediates, products, and the transition states connecting these species are identified and characterized. Geometries and harmonic frequencies are optimized by density functional theory at the B3LYP[27]/cc-pVTZ level. The energies are refined by the coupled cluster[28] CCSD(T)/cc-pVDZ with B3LYP/cc-pVTZ zero-point energy corrections. B3LYP/cc-pVTZ//CCSD(T)/cc-pVTZ level of calculation are expected to have an accuracy within 9 kJ mol^{-1}.[29] The GAUSSIAN09 program[30] is used in these electronic structure calculations.

Conflict of interest

The authors declare no conflict of interest.

[1] A. G. G. M. Tielens, *Annu. Rev. Astron. Astrophys.* **2008**, *46*, 289.

[2] A. M. Ricks, G. E. Douberly, M. A. Duncan, *Astrophys. J.* **2009**, *702*, 301.

[3] Y. M. Rhee, T. J. Lee, M. S. Gudipati, L. J. Allamandola, M. Head-Gordon, *Proc. Natl. Acad. Sci. USA* **2007**, *104*, 5274.

[4] K. Johansson, M. Head-Gordon, P. Schrader, K. Wilson, H. Michelsen, *Science* **2018**, *361*, 997.

[5] R. Gredel, *Astron. Astrophys.* **1999**, *351*, 657.

[6] A. G. G. M. Tielens, *Rev. Mod. Phys.* **2013**, *85*, 1021.

[7] a) D. S. Parker, R. I. Kaiser, T. P. Troy, M. Ahmed, *Angew. Chem. Int. Ed.* **2014**, *53*, 7740; *Angew. Chem.* **2014**, *126*, 7874;

Angew. Chem. Int. Ed. **2019**, *58*, 17442–17450

© 2019 Wiley-VCH Verlag GmbH & Co. KGaA, Weinheim

www.angewandte.org **17449**

b) D. S. N. Parker, R. I. Kaiser, B. Bandyopadhyay, O. Kostko, T. P. Troy, M. Ahmed, *Angew. Chem. Int. Ed.* **2015**, *54*, 5421; *Angew. Chem.* **2015**, *127*, 5511; c) T. Yang, R. I. Kaiser, T. P. Troy, B. Xu, O. Kostko, M. Ahmed, A. M. Mebel, M. V. Zagidullin, V. N. Azyazov, *Angew. Chem. Int. Ed.* **2017**, *56*, 4515; *Angew. Chem.* **2017**, *129*, 4586.

[8] M. Frenklach, E. D. Feigelson, *Astrophys. J.* **1989**, *341*, 372.

[9] H. Wang, M. Frenklach, *Combust. Flame* **1997**, *110*, 173.

[10] T. Yang, T. P. Troy, B. Xu, O. Kostko, M. Ahmed, A. M. Mebel, R. I. Kaiser, *Angew. Chem. Int. Ed.* **2016**, *55*, 14983; *Angew. Chem.* **2016**, *128*, 15207.

[11] L. Zhao, R. I. Kaiser, B. Xu, U. Ablikim, M. Ahmed, D. Joshi, G. Veber, F. R. Fischer, A. M. Mebel, *Nat. Astron.* **2018**, *2*, 413.

[12] L. Zhao, et al., *J. Phys. Chem. Lett.* **2018**, *9*, 2620.

[13] L. Zhao, R. I. Kaiser, B. Xu, U. Ablikim, M. Ahmed, M. M. Evseev, E. K. Bashkirov, V. N. Azyazov, A. M. Mebel, *Nat. Astron.* **2018**, *2*, 973.

[14] H. Jin, A. Frassoldati, Y. Wang, X. Zhang, M. Zeng, Y. Li, F. Qi, A. Cuoci, T. Faravelli, *Combust. Flame* **2015**, *162*, 1692.

[15] B. Shukla, A. Susa, A. Miyoshi, M. Koshi, *J. Phys. Chem. A* **2008**, *112*, 2362.

[16] S. Xiong, J. Li, J. Wang, Z. Li, X. Li, *Comput. Theor. Chem.* **2012**, *985*, 1.

[17] D. Bauich, et al., *J. Phys. Chem. Ref. Data* **1992**, *21*, 411.

[18] S. Hino, K. Seki, H. Inokuchi, *Chem. Phys. Lett.* **1975**, *36*, 335.

[19] R. Boschi, E. Clar, W. Schmidt, *J. Chem. Phys.* **1974**, *60*, 4406.

[20] Y. Ling, C. Lifshitz, *J. Phys. Chem.* **1995**, *99*, 11074.

[21] A. C. Brown, J. Gibson, *J. Chem. Soc. Trans.* **1892**, *61*, 367.

[22] M. Shibuya, M. Kato, M. Ozawa, P. H. Fang, E. Osawa, *Fullerene Sci. Technol.* **1999**, *7*, 181.

[23] M. Otsuka, F. Kemper, J. Cami, E. Peeters, J. Bernard-Salas, *Mon. Not. R. Astron. Soc.* **2014**, *437*, 2577.

[24] F. J. Lovas, R. J. McMahon, J.-U. Grabow, M. Schnell, J. Mack, L. T. Scott, R. L. Kuczkowski, *J. Am. Chem. Soc.* **2005**, *127*, 4345–4349.

[25] F. Zhang, R. I. Kaiser, V. V. Kislov, A. M. Mebel, A. Golan, M. Ahmed, *J. Phys. Chem. Lett.* **2011**, *2*, 1731.

[26] F. Qi, *Proc. Combust. Inst.* **2013**, *34*, 33.

[27] a) A. D. Becke, *J. Chem. Phys.* **1992**, *96*, 2155; b) A. D. Becke, *J. Chem. Phys.* **1992**, *97*, 9173; c) A. D. Becke, *J. Chem. Phys.* **1993**, *98*, 5948; d) C. Lee, W. Yang, R. G. Parr, *Phys. Rev. B* **1988**, *37*, 785.

[28] a) G. D. Purvis III, R. J. Bartlett, *J. Chem. Phys.* **1982**, *76*, 1910; b) C. Hampel, K. A. Peterson, H.-J. Werner, *Chem. Phys. Lett.* **1992**, *190*, 1; c) P. J. Knowles, C. Hampel, H. J. Werner, *J. Chem. Phys.* **1993**, *99*, 5219; d) M. J. Deegan, P. J. Knowles, *Chem. Phys. Lett.* **1994**, *227*, 321.

[29] M. Förstel, P. Maksyutenko, B. Jones, B.-J. Sun, A. Chang, R. Kaiser, *Chem. Commun.* **2016**, *52*, 741.

[30] M. J. Frisch, et al., Gaussian 09, Revision A.1 Gaussian Inc., Wallingford CT **2009**.